ANL/CSE-13/7

Speciation and Concentrations of Metals in a Homogeneous Reactor Fuel Solution

Chemical Science and Engineering Division

About Argonne National Laboratory
Argonne is a U.S. Department of Energy laboratory managed by UChicago Argonne, LLC under contract DE-AC02-06CH11357. The Laboratory's main facility is outside Chicago, at 9700 South Cass Avenue, Argonne, Illinois 60439. For information about Argonne and its pioneering science and technology programs, see www.anl.gov.

DOCUMENT AVAILABILITY

Online Access: U.S. Department of Energy (DOE) reports produced after 1991 and a growing number of pre-1991 documents are available free via DOE's SciTech Connect (http://www.osti.gov/scitech/)

Reports not in digital format may be purchased by the public from the National Technical Information Service (NTIS):
U.S. Department of Commerce
National Technical Information Service
5301 Shawnee Rd
Alexandra, VA 22312
www.ntis.gov
Phone: (800) 553-NTIS (6847) or (703) 605-6000
Fax: (703) 605-6900
Email: **orders@ntis.gov**

Reports not in digital format are available to DOE and DOE contractors from the Office of Scientific and Technical Information (OSTI):
U.S. Department of Energy
Office of Scientific and Technical Information
P.O. Box 62
Oak Ridge, TN 37831-0062
www.osti.gov
Phone: (865) 576-8401
Fax: (865) 576-5728
Email: **reports@osti.gov**

Disclaimer
This report was prepared as an account of work sponsored by an agency of the United States Government. Neither the United States Government nor any agency thereof, nor UChicago Argonne, LLC, nor any of their employees or officers, makes any warranty, express or implied, or assumes any legal liability or responsibility for the accuracy, completeness, or usefulness of any information, apparatus, product, or process disclosed, or represents that its use would not infringe privately owned rights. Reference herein to any specific commercial product, process, or service by trade name, trademark, manufacturer, or otherwise, does not necessarily constitute or imply its endorsement, recommendation, or favoring by the United States Government or any agency thereof. The views and opinions of document authors expressed herein do not necessarily state or reflect those of the United States Government or any agency thereof, Argonne National Laboratory, or UChicago Argonne, LLC.

ANL/CSE-13/7

Speciation and Concentrations of Metals in a Homogeneous Reactor Fuel Solution

by
J. Jerden, J. Kropf, A. Bakel, and G. Vandergrift
Chemical Science and Engineering Division, Argonne National Laboratory

prepared for
U.S. Department of Energy, National Nuclear Security Administration,
Office of Defense Nuclear Nonproliferation

September 30, 2009

CONTENTS

1 INTRODUCTION 1

1.1 Background 1
1.2 Report Contents 1
1.3 Summary of Results 1

2 MOLYBDENUM SPECIATION IN THE MIPS FUEL 3

2.1 Introduction 3
2.2 Process Used to Add Molybdenum Species to the GWB Database 3
2.3 Results 3

3 X-RAY ABSORPTION EXPERIMENTS ON MOLYBDENUM SOLUTIONS AND MOLYBDENUM ADSORBED TO TITANIA AND ALUMINA SORBENTS 9

3.1 Introduction 9
3.2 Summary 9
3.3 Experiment 9
3.4 Sorbents 10
3.5 X-ray Absorption Measurements 10
3.6 Results 10

4 THE pH EFFECT OF NO(g), N_2(g), AND H_2O(g) LOSS FROM A 1 MOLAR URANYL NITRATE, 0.1 MOLAR HNO_3 SOLUTION AT 80°C: EQUILIBRIUM MODELS 16

4.1 Introduction 16
4.2 Results and Discussion 16
4.2.1 Modeling Scenarios 19
4.3 List of Selected Reactions 19

5 PRELIMINARY RESULTS FROM URANYL PEROXIDE PRECIPITATION EXPERIMENTS 24

5.1 Introduction 24
5.2 Experiment 24
5.3 Preliminary Experimental Results 24
5.4 Modeling Results 25

6 CONCLUSION 28

7 REFERENCES 29

FIGURES

1 Molybdenum Speciation Using $\log_{10}K = -4.24$ for the Reaction $HMoO_4^- \leftrightarrow MoO_4^{2-} + H^+$ 5

2 Molybdenum Speciation Using $\log_{10}K = -9.67$ for the Reaction $HMoO_4^- \leftrightarrow MoO_4^{2-} + H^+$ 7

3 Molybdenum Speciation Using $\log_{10}K = -4.24$ for the Reaction $HMoO_4^- \leftrightarrow MoO_4^{2-} + H^+$ 8

4 XANES Plot Comparing Adsorbed Mo Spectra to MoO_2 and MoO_3 11

5 XANES Plot Comparing Mo Solution Spectra to MoO_2 and MoO_3 11

6 Imaginary Component of the FT between 3.0 and 15.5 $Å^{-1}$ for the Three Solution Samples: pH 0, 1, and 2 13

7 pH 0 Solution with the Best Fit..... 13

8 Imaginary Component of the FT for Three Similar Adsorbed Mo Species 14

9 FT Magnitude for Five Adsorbed Mo Species 15

10 Fit Mo Adsorbed to TSM..... 15

11 N_2(g) “Negative” Titration..... 17

12 NO(g) “Negative” Titration 18

13 H_2O(g) “Negative” Titration..... 20

14 Redox Relationships between Species..... 21

15 Activity Diagram Showing the Stability Field of Uranyl Peroxide as a Function of H_2O_2 concentration and pH 26

16 Solid and Aqueous Speciation Diagrams for 1×10^{-3} M and 1×10^{-6} M H_2O_2 Steady-State Concentration..... 27

TABLES

1 Free Energy of Reaction and Equilibrium Constants for Selected Basis Reactions Used for Calculating Molybdenum Speciation 4

2 Nearest-Neighbor Bond Lengths and Coordination Numbers for Mo Solutions 12

3 Concentrations and Experimental Conditions for Uranyl Peroxide Stability Tests 25

SPECIATION AND CONCENTRATIONS OF METALS IN A HOMOGENEOUS REACTOR FUEL SOLUTION

1 INTRODUCTION

1.1 BACKGROUND

Argonne National Laboratory scientists and engineers are collaborating with personnel from Babcock and Wilcox (B&W) to help optimize the design of their Medical Isotope Production System (MIPS). The major components of the MIPS are a homogeneous solution reactor containing low-enriched uranyl nitrate fuel, a molybdenum extraction system consisting of anion exchange columns, and an off-gas treatment facility. The MIPS project is of high priority because it would provide an industrial-scale domestic source of medical isotopes that is not currently available.

1.2 REPORT CONTENTS

This report presents results from four different studies performed in fiscal year (FY) 2009 at Argonne. The purpose of these studies was to develop a better understanding of the speciation and concentrations of key elements in the MIPS reactor fuel. The results discussion provides information that can be used to help optimize reactor operation and enhance the efficiency with which molybdenum is extracted from the irradiated low-enriched uranium (LEU) fuel solution.

The four studies cover (1) speciation calculations for molybdenum within the reactor fuel, (2) x-ray absorption experiments that investigate the molecular structure of molybdenum in relevant solutions and adsorbed to relevant sorbents, (3) thermodynamic modeling of how the pH of the reactor solution may change due to the loss of nitrogen through the radiolytic destruction of nitrate, and (4) modeling and experimental work that look at the consequences of hydrogen peroxide production during reactor operation.

1.3 SUMMARY OF RESULTS

The key results from the molybdenum speciation calculations (Study 1) are that the cationic species MoO_4^{2+} is dominant below a pH of 0.8, while H_2MoO_4 is dominant at a pH of 0.8–3. At a pH of more than 3, $HMoO_4^-$ and MoO_4^{2-} are the dominant species. This study also notes that due to inconsistencies in the thermodynamic constants for molybdenum species over the pH range of interest, more experimental data are needed to verify the results. Knowing the molybdenum speciation in the MIPS fuel is important for understanding and optimizing the molybdenum extraction system.

The key results from the x-ray absorption experiments (Study 2) are that molybdenum in sodium nitrate solutions (surrogates for the MIPS fuel) are bound to at least 4 mol of oxygen

(two short bond lengths [~1.7 Å] and two longer ones [~2.2 Å]) and that the Mo-O bond lengths increase with increasing pH (samples with a pH of 0, 1, and 2 were analyzed). These results are preliminary, and some Mo-O or Mo-NO_3^- bonds may not be resolved in the current data set. More work is thus needed to resolve the uncertainties; however, the findings are useful in confirming the speciation of molybdenum under relevant condition.

The x-ray absorption results that look at the molecular structure of molybdenum adsorbed to the four sorbents being considered for the MIPS are difficult to interpret since they are not amenable to a unique fitting solution. However, the data suggest that the adsorbed Mo species are all fairly similar on the titania-based sorbents and different for the alumina sorbent. The data show that Mo-O bonds are approximately 1.7 Å (for all sorbents), and there appears to be a Mo-Ti distance of 3.5 Å for the titania sorbents. The precise structure of the adsorbed molybdenum, however, has not yet been resolved. Assuming that the Mo-Ti distance is correct, the results indicate that the molybdenum is adsorbed as an inner sphere complex (tightly bound) on the titania sorbents. The absence of a Mo-Al distance for the alumina sorbent suggests that molybdenum is bound as an outer sphere complex (weakly bound) on this material.

The key recommendation from the pH study (Study 3) is that we need to understand the system better before the pH model presented in this report can be used as supporting evidence for a process to adjust the pH during reactor operation. Further, when the results of this model are presented, a qualification should be added, stating that the results are semiquantitative (i.e., a “step” toward understanding the real system). The next step in understanding the pH variation during reactor operation would be to perform experiments in which the pH is measured during irradiation of a stimulant of the MIPS fuel. Such experiments are currently being planned by Argonne and B&W staff.

The key results from the hydrogen peroxide study (Study 4) are that a uranyl peroxide solid may form under certain conditions (depending on the steady-state concentration of H_2O_2 during reactor operation). However, due to the rate of destruction of H_2O_2 at relevant temperatures (e.g., 80°C), it is likely that the fuel solution will remain undersaturated with respect to uranyl peroxide as long as the solution pH remains lower than 2. But again, more experimental data are needed to verify these findings.

2 MOLYBDENUM SPECIATION IN THE MIPS FUEL

2.1 INTRODUCTION

The software "Geochemist's Workbench" (GWB) was used to model the speciation of molybdenum in uranyl nitrate and sodium nitrate as a function of pH and the concentration of molybdenum. For some model runs, molybdenum minerals were allowed to precipitate, and in other cases, precipitation was inhibited.

2.2 PROCESS USED TO ADD MOLYBDENUM SPECIES TO THE GWB DATABASE

Incorporating the molybdenum data into the database required the following four steps:

1. Tabulating the free energies of formation (G^o_f) for species of interest as well as for auxiliary species that are used to write the basis reactions.

2. Writing the basis reactions (Table 1). These reactions are used by the code to solve a matrix of mass and charge balance equations, which feed into an iterative algorithm that converges on a unique equilibrium state for the multiphase, multicomponent system of interest.

3. Calculating the free energy of reaction for the basis reactions (ΔG^o_r) by using the following equation: $\Delta G^o_r = \Sigma n_i G^o_{fi}$ (products) – $\Sigma n_i G^o_{fi}$ (reactants), where n_i is the molar coefficient of species i in the reaction.

4. Calculating the equilibrium constants (K) for the basis reactions by using the following relationships: $\Delta G^o_r = -RT\ln K$; therefore, $\log_{10}K = -\Delta G^o_r/2.303RT$. (The code uses $\log_{10}K$ values in its algorithms.) The basis reactions include redox transitions, which are written by using O_2(aq) in the place of e^- (Table 1).

2.3 RESULTS

There is no consensus in the literature for the value of the equilibrium constant for the reaction $HMoO_4^- \leftrightarrow MoO_4^{2-} + H^+$. This reaction plays a key role in determining molybdenum speciation at a low pH. When values of –4.24 or –3.89 are used (these values agree most closely with experimental results), the dominant molybdenum species are predicted to be MoO_4^{2+} and H_2MoO_4(aq) at a pH of <3. At 1×10^{-4} mol of molybdenum, the solution is saturated with respect to MoO_3 at a pH of 0.5–2.5. Also, at this concentration, the molybdenum polymer $Mo_7O_{21}^{6-}$ becomes a significant species at a pH of 3. At 1×10^{-3} mol of molybdenum, other polymers become dominant species: $Mo_7O_{22}(OH)_2^{4-}$ at a pH of 1–2 and $Mo_7O_{21}^{6-}$ at a pH of 2–4. Figures 1, 2, and 3 (and their captions) elaborate on the results.

TABLE 1 Free Energy of Reaction and Equilibrium Constants for Selected Basis Reactions Used for Calculating Molybdenum Speciation

Basis Reactions	ΔG^o_r (kJ/mol)	$\log_{10}K$	Source
$Mo_{metal} + 1.5O_2(aq) + H_2O \leftrightarrow MoO_4^{2-} + 2H^+$	–626.18	109.68	Bard et al. 1985
$Mo^{3+} + 0.75O_2(aq) + 2.5H_2O \leftrightarrow MoO_4^{2-} + 5H^+$	–200.32	35.09	Faure 1998
$MoO_2^+ + 0.25O_2(aq) + 1.5H_2O \leftrightarrow MoO_4^{2-} + 3H^+$	26.87	–4.71	Faure 1998
$MoO_2^{2+} + 2H_2O \leftrightarrow MoO_4^{2-} + 4H^+$	49.37	–8.65	Lindsay 1979
$HMoO_4^- \leftrightarrow MoO_4^{2-} + H^+$	55.20	–9.67	Faure 1998
$HMoO_4^- \leftrightarrow MoO_4^{2-} + H^+$	24.20	–4.24	Lindsay 1979
$HMoO_4^- \leftrightarrow MoO_4^{2-} + H^+$	22.20	–3.89	Baes and Mesmer 1976
$H_2MoO_4(aq) \leftrightarrow MoO_4^{2-} + 2H^+$	44.3	–7.76	Bard et al. 1985
$H_2MoO_4(aq) \leftrightarrow MoO_4^{2-} + 2H^+$	42.81	–7.50	Baes and Mesmer 1976
$Mo_7O_{24}^{6-} + 4H_2O \leftrightarrow 7MoO_4^{2-} + 8H^+$	329.58	–57.74	Baes and Mesmer 1976
$Mo_7O_{23}(OH)^{5-} + 4H_2O \leftrightarrow 7MoO_4^{2-} + 9H^+$	354.70	–62.14	Baes and Mesmer 1976
$Mo_7O_{22}(OH)_2^{4-} + 4H_2O \leftrightarrow 7\ MoO_4^{2-} + 10\ H^+$	374.90	–65.68	Baes and Mesmer 1976
$Mo_7O_{21}(OH)_3^{3-} + 4H_2O \leftrightarrow 7MoO_4^{2-} + 11H^+$	389.34	–68.21	Baes and Mesmer 1976
$Mo_{19}O_{59}^{4-} + 17H_2O \leftrightarrow 19MoO_4^{2-} + 34H^+$	1120.48	–196.3	Baes and Mesmer 1976
$MoO_2(c) + 0.5O2(aq) + H_2O \leftrightarrow MoO_4^{2-} + 2H^+$	–76.62	13.42	Bard et al. 1985
$MoO_3(c) + H_2O \leftrightarrow MoO_4^{2-} + 2H^+$	99.70	–12.51	Faure 1998
$Mo_3O_8(c) \leftrightarrow MoO_4^{2-} + 2MoO^{2+}$	142.23	–24.91	Bard et al. 1985
$Mo_4O_{11}(c) + H2O \leftrightarrow 2MoO_4^{2-} + 2MoO^{2+} + 2H^+$	44.55	–7.80	Bard et al. 1985
$H_2MoO_4(c) \leftrightarrow MoO_4^{2-} + 2H^+$	73.5	–12.87	Bard et al. 1985

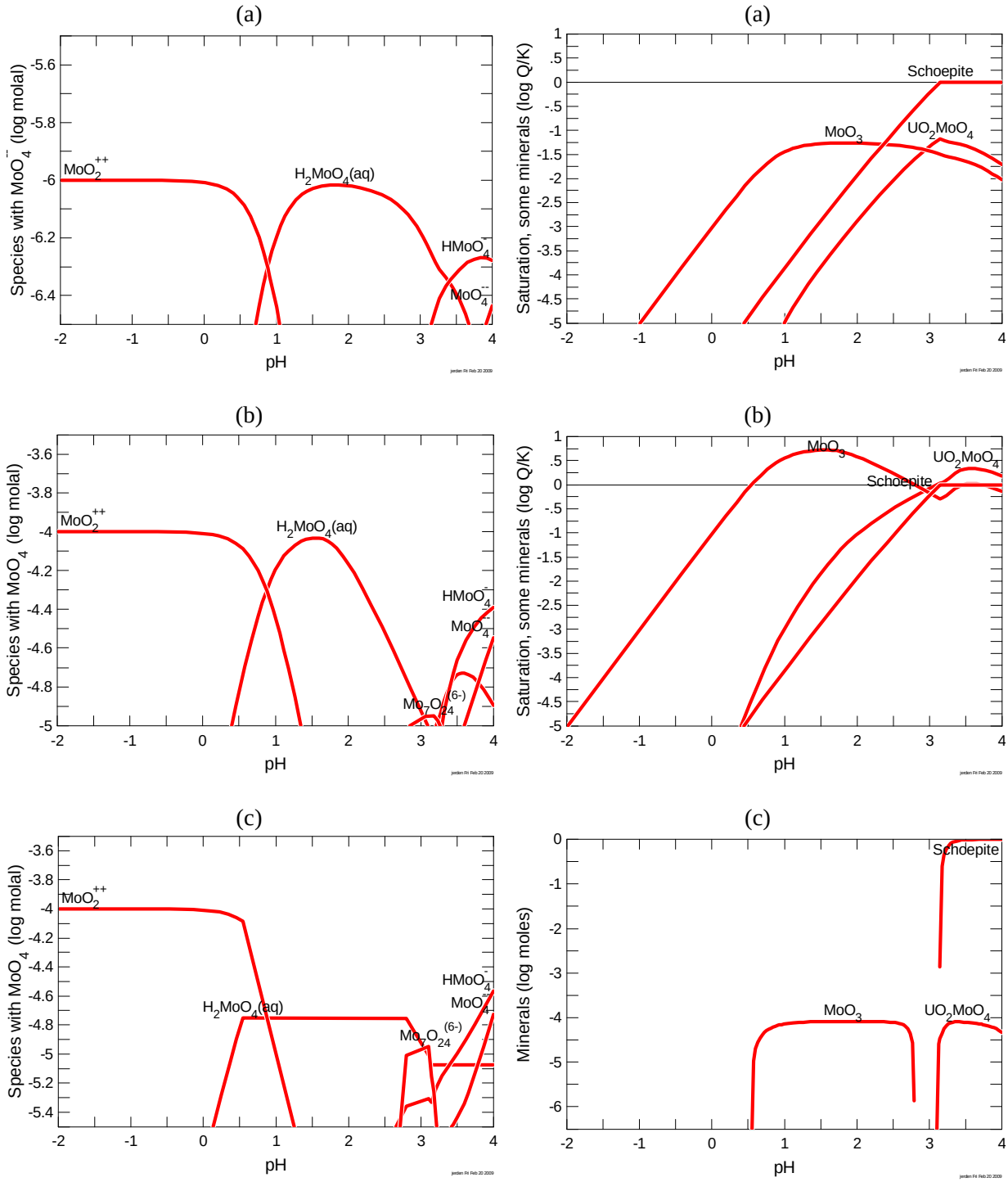

FIGURE 1 Molybdenum Speciation Using $\log_{10}K = -4.24$ for the Reaction $HMoO_4^- \leftrightarrow MoO_4^{2-} + H^+$ [Schoepite = uranyl oxide hydrate. (a) 1×10^{-6} molar Mo_{total}: The solution is undersaturated with respect of molybdenum minerals. (b) 1×10^{-4} molar Mo_{total}: The solution is supersaturated with respect to molybdenum minerals (precipitation inhibited). (c) 1×10^{-4} molar Mo_{total}: The solution is saturated with respect to molybdenum minerals (precipitation allowed). Note the prevalence of polymeric species $Mo_7O_{21}^{6-}$ at a pH of 3.]

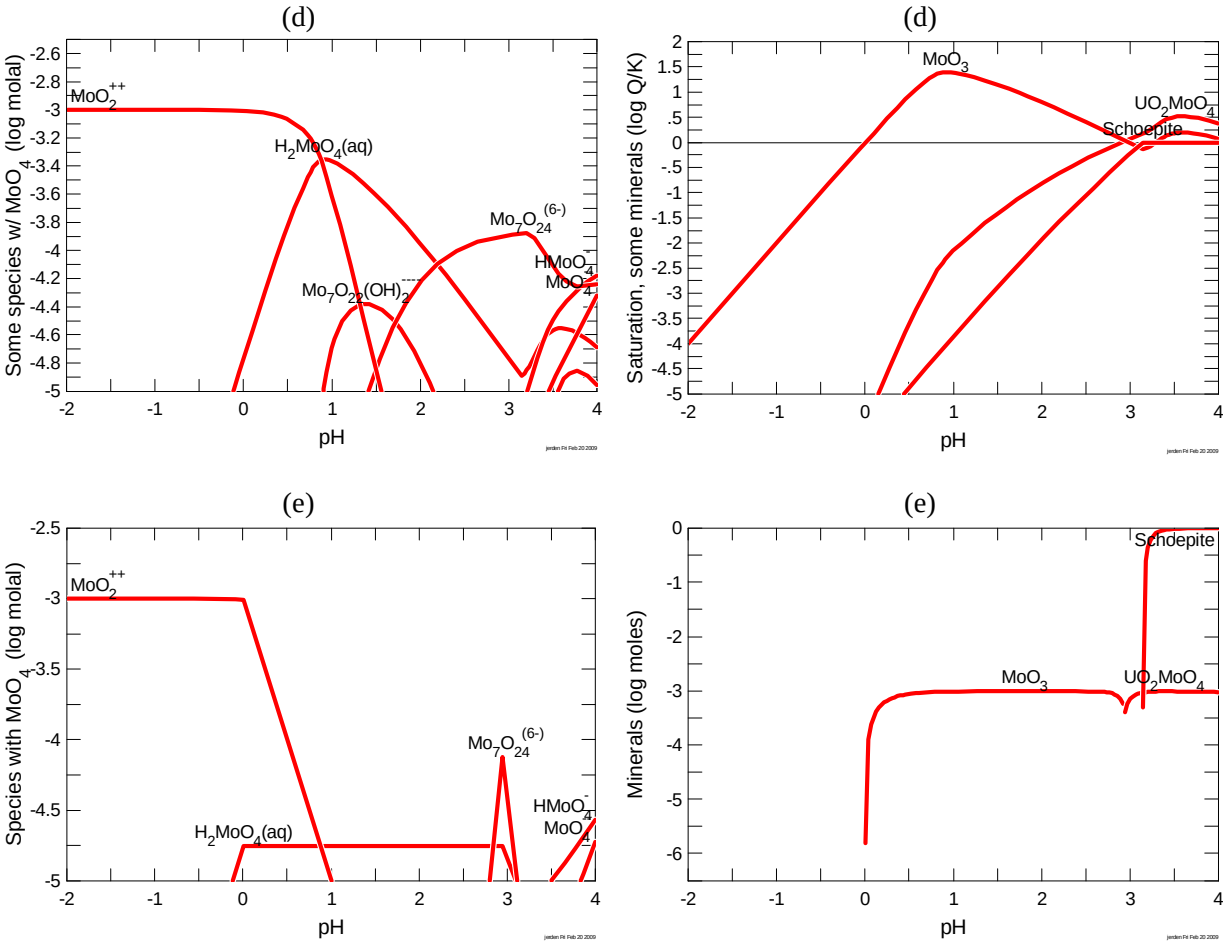

FIGURE 1 (Cont.) [(d) 1 × 10^{-3} molar Mo_{total}: The solution is supersaturated with respect to molybdenum minerals (precipitation inhibited). Note the prevalence of polymeric species $Mo_7O_{22}(OH)_2^{4-}$ at a pH of 1–2 and $Mo_7O_{21}^{6-}$ at a pH of 2–4. (e) 1 × 10^{-3} molar Mo_{total}: The solution is saturated with respect to molybdenum minerals (precipitation allowed).]

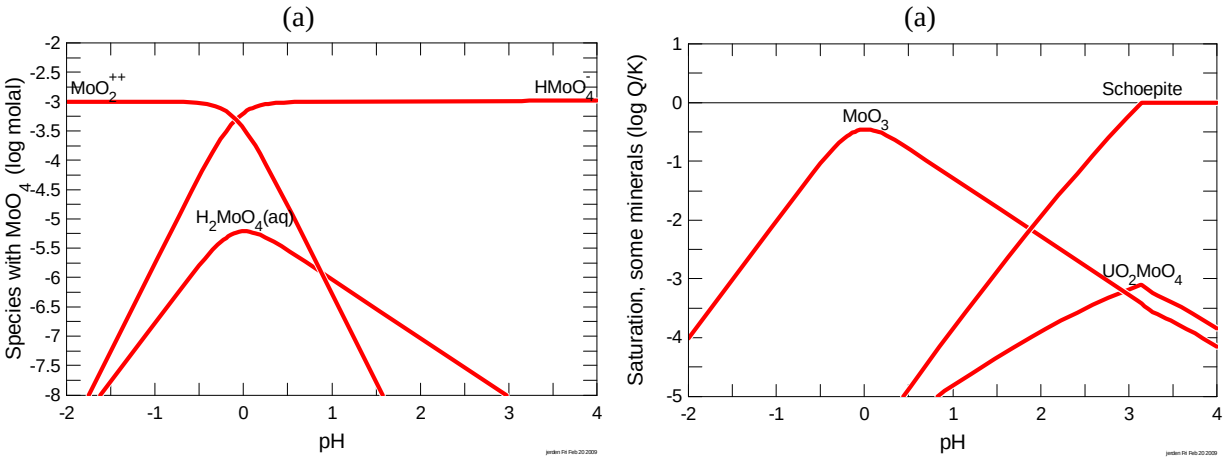

FIGURE 2 Molybdenum Speciation Using $\log_{10}K = -9.67$ for the Reaction $HMoO_4^- \leftrightarrow MoO_4^{2-} + H^+$ [Schoepite = uranyl oxide hydrate. (a) 1×10^{-3} molar Mo_{total}: Even at this high concentration, the solution is undersaturated with respect to molybdenum minerals; this does not agree with experimental results. Therefore, the equilibrium constant $\log_{10}K = -4.24$ or -3.89 is deemed more accurate than -9.67.]

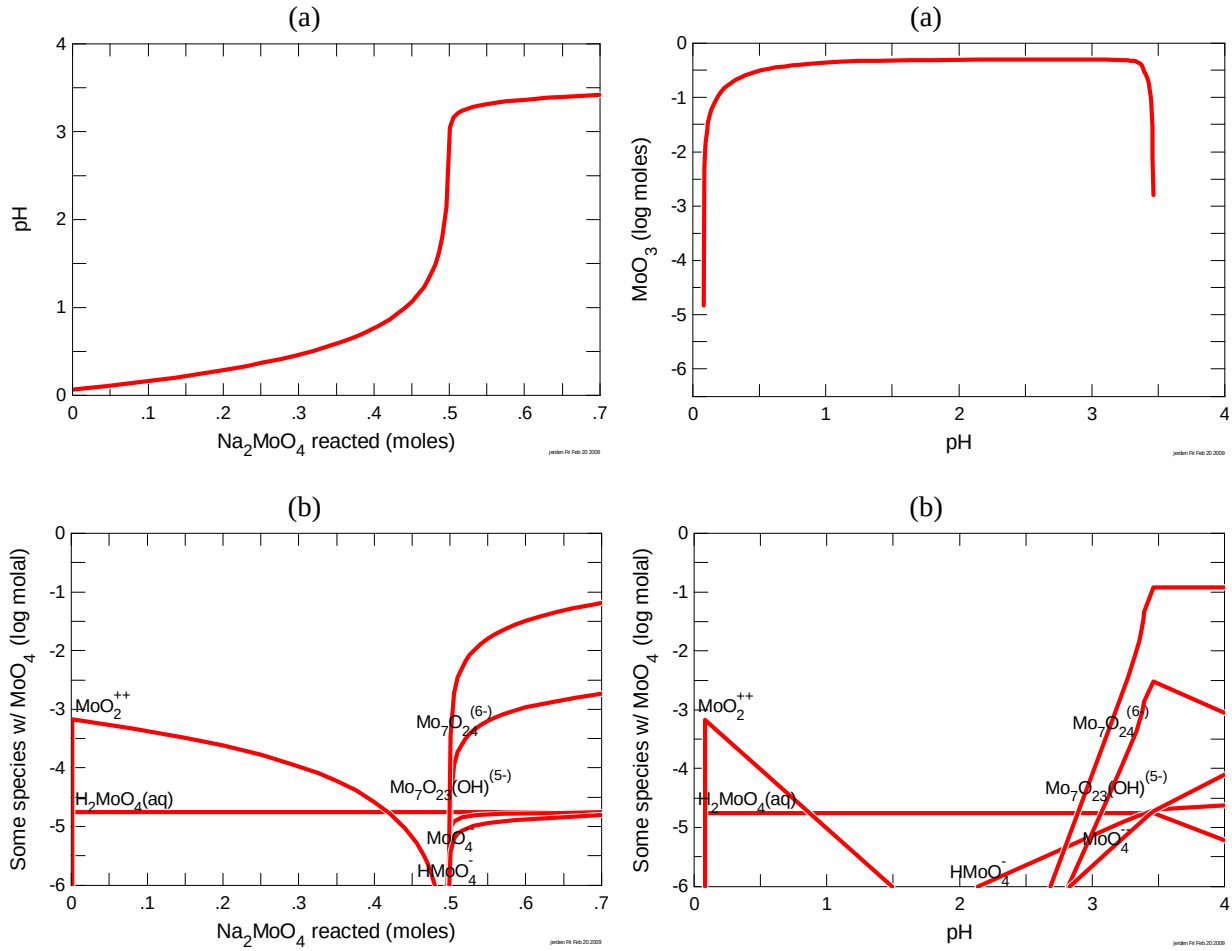

FIGURE 3 Molybdenum Speciation Using $\log_{10}K = -4.24$ for the Reaction $HMoO_4^- \leftrightarrow MoO_4^{2-} + H^+$ [For this model, Na_2MoO_4 is titrated into a solution of 1 molar $NaNO_3$. (a) Curves showing how pH changes with the addition of sodium molybdate and the amount of molybdenum oxide that precipitates. (b) Molybdenum speciation as a function of sodium molybdate added and pH.]

3 X-RAY ABSORPTION EXPERIMENTS ON MOLYBDENUM SOLUTIONS AND MOLYBDENUM ADSORBED TO TITANIA AND ALUMINA SORBENTS

3.1 INTRODUCTION

The purpose of these experiments was to determine the molecular structure of molybdenum in solutions simulating the MIPS fuel and to try to constrain the mechanism by which molybdenum is adsorbing the sorbents being considered for molybdenum extraction from the MIPS fuel. The results will help us understand the chemistry of molybdenum under conditions relevant to the MIPS and thus help optimize the system for molybdenum extraction. Both extended x-ray absorption fine structure (EXAFS) and x-ray absorption near edge structure (XANES) techniques were used.

3.2 SUMMARY

Two sets of experiments were conducted to determine Mo speciation in solution at different pHs and to determine Mo speciation or interaction with the support for various sorbent materials. The results for the solutions indicate that the Mo oxidation state is very close to, but not entirely, +6, with a tetrahedral nearest-neighbor Mo-O coordination environment including two short Mo-O bonds from 1.69 to 1.73 Å. (Note that since there is no explanation chemically for Mo reduction in these samples, the presence of an oxidation state lower than +6 is likely due to reduction in the x-ray beam; however, further work is needed to confirm this hypothesis.) The results for the adsorbed Mo indicate that there is some dependence of the coordination environment on the support, but that the Mo is entirely in the +6 oxidation state. The adsorbed Mo species has two short Mo-O bonds, but these are slightly longer, at 1.74–1.76 Å. In both cases, the angle between the short Mo-O bonds is not close to 180°, which is indicated by the absence of significant multiple-scattering peaks in the EXAFS Fourier transform (FT).

3.3 EXPERIMENT

For the solution experiments, Na_2MoO_4 powder was dissolved in nitric acid diluted to a pH of 0, 1, and 2 by using deionized water. The concentration of each sample was 1×10^{-4} molar, as determined by the mass of sodium molybdate dissolved. After each solution was stirred for 24 hours at 25°C, approximately 1 mL of each solution was placed in a clear plastic cuvette for x-ray absorption analyses.

For the sorbent experiments, 10 mL of sodium molybdate solution containing 5×10^{-3} M molybdenum was reacted with 10 mg of each sorbent for 24 hours at 25°C. The molybdate solutions were prepared by dissolving Na_2MoO_4 powder in nitric acid diluted to a pH of 1 with deionized water.

3.4 SORBENTS

The sorbents used in these experiments are discussed in detail in a 2009 unpublished report by Stepinski and others sent to B&W. The sorbents being evaluated at Argonne for use in the extraction of Mo-99 from the MIPS fuel consist of nanocrystalline titania and alumina. The sorbent referred to as T-52 (labeled TS2 in figures) consists of 25 mol% of SnO_2 and 75 mol% TiO_2, T-5M (labeled TSM in figures) consists of 5 mol% of ZrO_2 and 95 mol% TiO_2, Sachtopore-80 (labeled SBO in figures) consists of nearly pure TiO_2, and the alumina sorbent is pure Al_2O_3. Pure anatase powder was also used in XAS experiments as a control.

3.5 X-RAY ABSORPTION MEASUREMENTS

Both sets of measurements were made at the MRCAT beamline 10ID at Argonne's Advanced Photon Source. The x-ray absorption fluorescence spectra (XAFS) for the solutions were measured in fluorescence mode by using the "Lytle" detector with soller slits and a 6-absorption-length zirconium metal filter. Krypton gas was used in the 6-cm ionization chamber.

The XAFS for the adsorbed species was measured by using a log spiral Laue crystal analyzer (BLA) tuned to the Mo K alpha fluorescence with two scintillation detectors. Due to the vastly different surface areas of the supports and perhaps other factors, the signal was a couple of orders of magnitude larger for Mo on some supports, so the beam size was decreased in order to keep the detectors close to their linear range.

For the solution samples, a simultaneous measurement of a metallic Mo foil spectrum was possible. The Mo edge was calibrated to 20,000.4 eV for the zero crossing of the second derivative signal corresponding to the lower energy maximum of the first derivative. For the adsorbed species, insufficient x-rays penetrated the entire length of the sample, so in that case, we relied on beamline stability to ensure that the energy calibration remained consistent. In the cases where a reference was measured, several spectra were aligned to the calibrated reference and merged to form the spectra analyzed. For the adsorbed Mo, the spectra for each sample were aligned to a chosen spectrum and then merged.

3.6 RESULTS

Figures 4 and 5 show the Mo XANES compared to MoO_2 and MoO_3 standards. These two standards give an indication of the typical edge energy for Mo(+4) and Mo(+6), although geometry effects may have a small impact on the edge position. The pre-edge peak at about 20,007 eV is a typical indication of the Mo(+6) oxidation state, based on this and other standard samples. In Figure 4, the pre-edge peak in the adsorbed Mo spectra is nearly identical to the MoO_3 standard, except for the sample with the alumina substrate, and all of the edges appear to be shifted slightly to higher energy. For the Mo solutions, shown in Figure 5, the pre-edge peak appears to be shifted slightly to lower energy, as is the edge. Both of these indicators suggest that although the Mo is primarily +6, some fraction with a lower oxidation state is likely. As there is

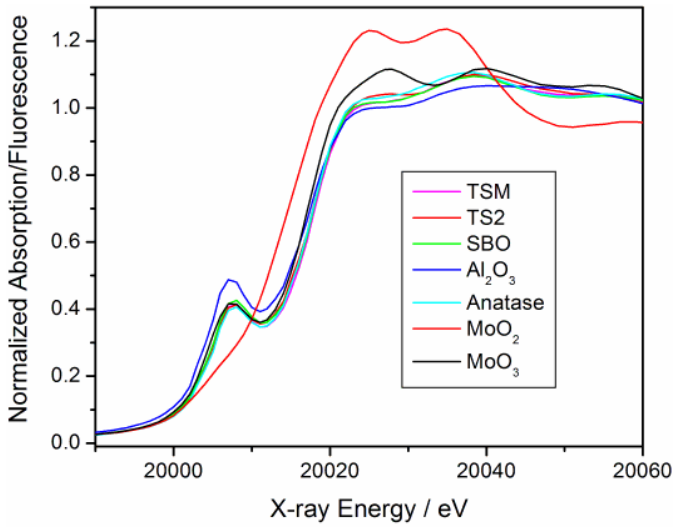

FIGURE 4 XANES Plot Comparing Adsorbed Mo Spectra to MoO_2 and MoO_3

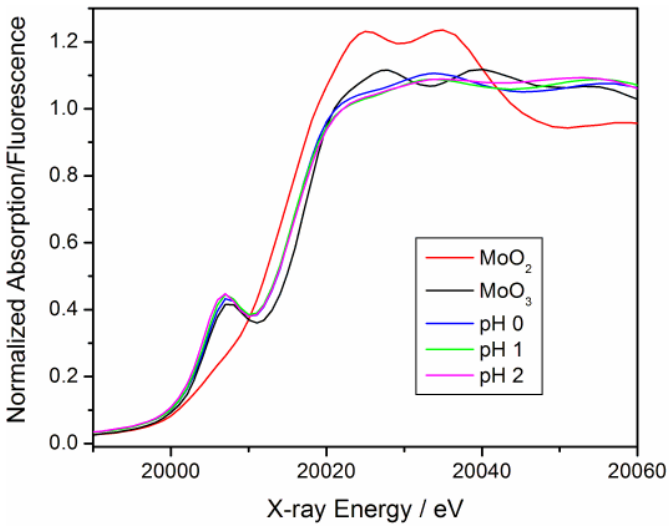

FIGURE 5 XANES Plot Comparing Mo Solution Spectra to MoO_2 and MoO_3

no explanation chemically for Mo reduction in these samples, the presence of an oxidation state lower than +6 is likely due to reduction in the x-ray beam; however, further work is needed to confirm this hypothesis.

Neither of the two standards, MoO_2 nor MoO_3, has similar nearest-neighbor Mo-O bond lengths. For MoO_2, there is a single length at 1.99 Å, but for MoO_3, there are two scattering paths, one at 1.66 Å and the second at 1.93 Å. These numbers are within 0.02 Å of those found in the calculations from crystallographic measurements.

The spectra for the Mo solutions exhibit a trend as a function of solution pH. The Mo-O bond length gets longer as the acidity of the solution decreases, although the XANES shows that the edge energy is the same. The pre-edge peak remains shifted to a slightly lower energy, perhaps indicating a small reduction of the average Mo valence.

The fit results are shown in Table 2. The coordination number is rounded to the nearest integer. The uncertainty is smaller than one unit, typically about 0.3, except for the pH 2 data, which is fit best with only one longer Mo-O bond but has a higher uncertainty. Figure 6 shows the imaginary component of the FT (not corrected for phase shift) for the three solutions. The purpose of showing the imaginary component rather than the magnitude is to more easily see the changes in bond length. In particular, the zero-crossing through about 1.3 Å shows that the pH 0 sample has a shorter bond length than the other two samples, which are about the same. The structure between 1.5 and 2.0 Å shows a larger shift between all three samples.

Although it is not surprising, there is no indication in the data for a linear or nearly linear arrangement of the two short Mo-O bonds. The absence of a strong multiple-scattering peak precludes a linear arrangement; furthermore, it limits the maximum angle between the bonds. This angle has not yet been estimated. The data also suggest the existence of a longer Mo-O scattering path. Figure 7 shows how difficult it is to obtain reliable fit results for the 2.0–2.6 Å region.

The adsorbed Mo species are all fairly similar, at least for the two short Mo-O bonds. These Mo-O are at about 1.73 Å. Again, there is no evidence of a linear or nearly linear O-Mo-O arrangement for the two short Mo-O bonds. The peak of the FT is shifted slightly to higher R in the adsorbed species, since there is not a bond at 2.2+/- Å to interfere with the short Mo-O scattering path.

Figure 8 indicates the similarity of the three spectra presented. For these three samples, it is reasonable to conclude that the Mo species are essentially the same, to the limit of the data quality. A peak is present at about 3.2 Å (as shown in Figure 8, not phase-shift corrected) that seems to be due to an interaction of Mo with the support. If this assumption is made, the Mo-Ti distance is about 3.50 Å, although there is significant spread in the best fit values (+/- 0.06 Å). It is also clear that in these samples, a third scattering path is present (as shown in Figure 8) with a peak at

TABLE 2 Nearest-Neighbor Bond Lengths and Coordination Numbers for Mo Solutions

Sample	N	R (Å)
pH 0	2	1.690 ± 0.010
	2	2.203 ± 0.013
pH 1	2	1.720 ± 0.010
	2	2.251 ± 0.015
pH 2	2	1.727 ± 0.008
	1	2.280 ± 0.020

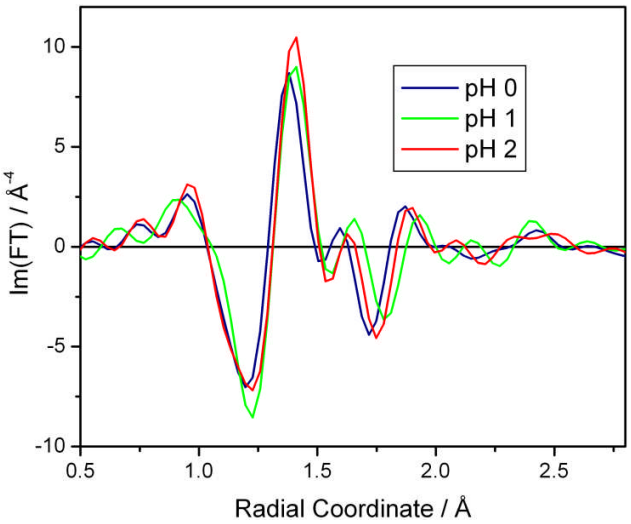

FIGURE 6 Imaginary Component of the FT between 3.0 and 15.5 Å^{-1} for the Three Solution Samples: pH 0, 1, and 2

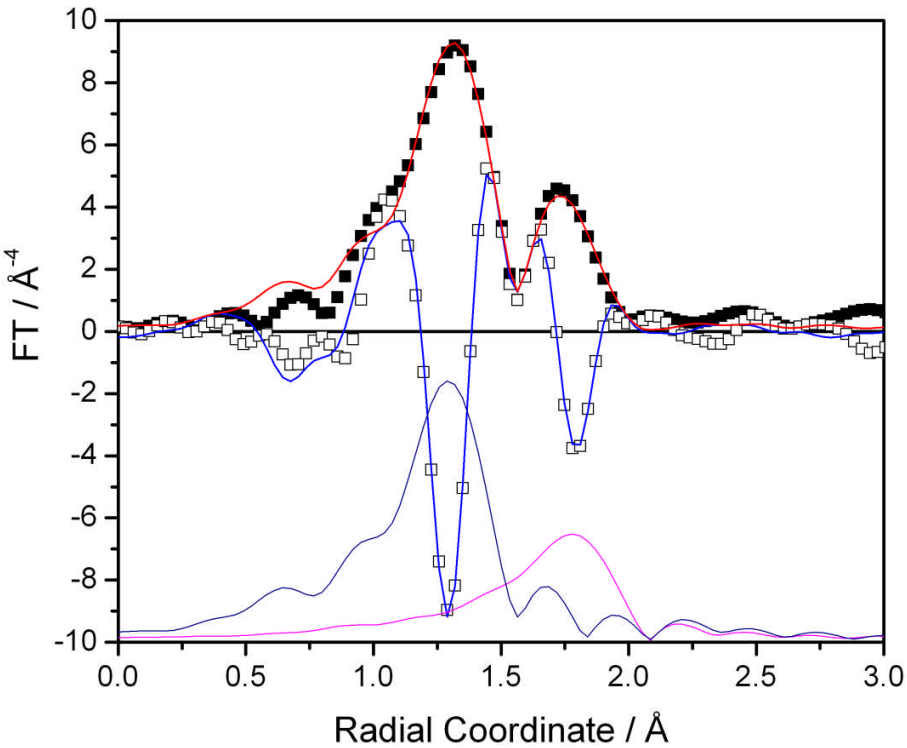

FIGURE 7 pH 0 Solution with the Best Fit (The experimental data are the symbols, and the fits are indicated by the red and blue lines. The traces along the bottom are the FT magnitudes of the individual scattering paths.)

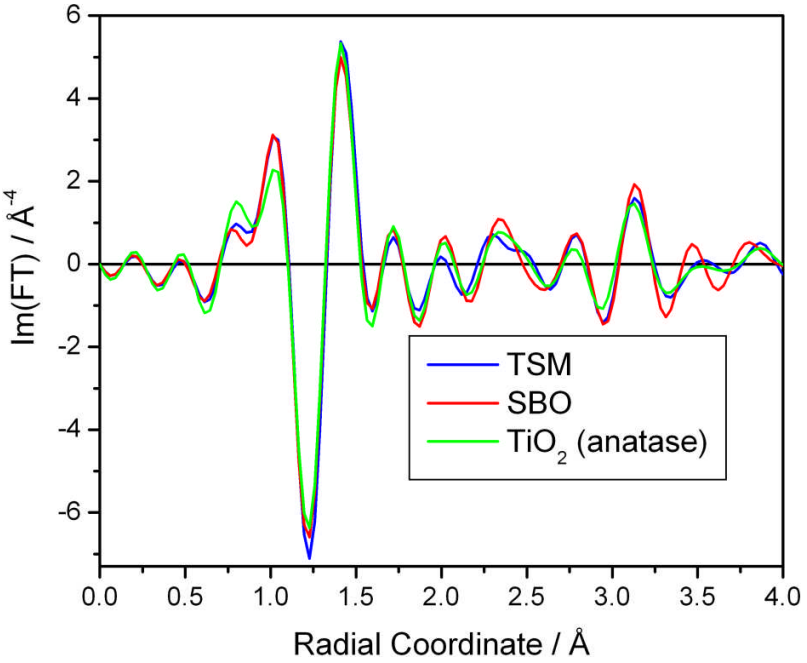

FIGURE 8 Imaginary Component of the FT for Three Similar Adsorbed Mo Species (*k* = 3.0–11.5 Å^{-1})

about 2.7 Å. This path is highly correlated with the presumed Mo-Ti path; therefore, it is not possible to unambiguously identify the element responsible for this path. Mo, Ti, and O all fit well, but O seems to be the best choice. This correlation also has the side effect of limiting the accuracy of all of the path parameters except for distance, and a coordination number cannot be measured reliably.

Figure 9 adds two spectra that are not similar. These are the samples with TS2 and alumina substrates. The interaction of Mo with the support is not visible in these two spectra. Figure 10 shows the fitting of adsorbed Mo on sorbent TSM.

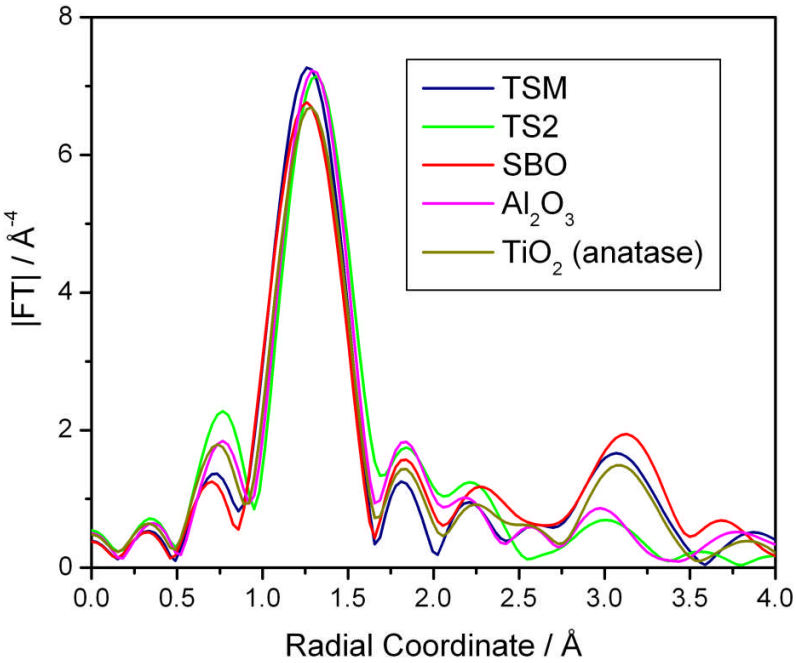

FIGURE 9 FT Magnitude for Five Adsorbed Mo Species (k = 3.0–11.5 Å^{-1})

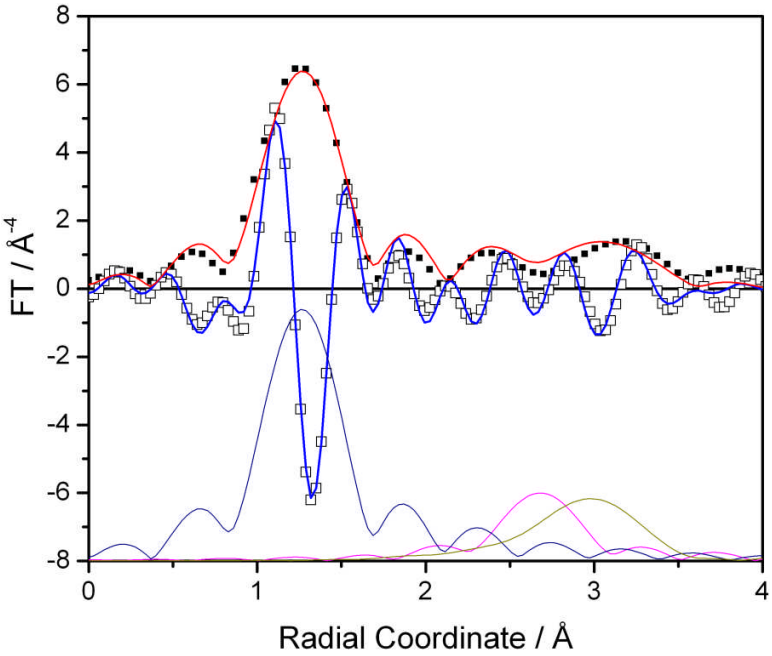

FIGURE 10 Fit Mo Adsorbed to TSM [k = 3.0–10.5 Å^{-1}. The three components of the fit are, from left to right on bottom axis: Mo-O (1.73 Å), Mo-O/Ti/Mo, and Mo-Ti (~3.50 Å).]

4 THE pH EFFECT OF NO(G), N_2(G), AND H_2O(G) LOSS FROM A 1 MOLAR URANYL NITRATE, 0.1 MOLAR HNO_3 SOLUTION AT 80°C: EQUILIBRIUM MODELS

4.1 INTRODUCTION

The pH calculations were made by using the thermodynamic codes OLI ESP and Release 3.0 of the GWB. Results from the two codes agree. The thermodynamic database used for modeling was compiled from the literature (Wolery and Daveler 1992). In general, both modeling codes use a Gibb's free energy minimization technique to determine the equilibrium state of the system of interest. More specifically, the codes use the equilibrium constants for a set of basis reactions to solve a matrix of mass and charge balance equations. Results from these calculations feed into an iterative algorithm that converges on a unique equilibrium state for the multicomponent, multiphase system of interest.

4.2 RESULTS AND DISCUSSION

Reactions a through c in this section are used by the thermodynamic modeling code to simulate how the loss of nitrogen or nitrogen oxide from the uranyl nitrate solution influences the pH. No radiolytic species can be incorporated into this model in its current configuration (it is strictly an equilibrium model). Therefore, the results should be viewed only as being perhaps informative but not as a mechanistic simulation of the process. In fact, we are concerned that in its current state, this pH model is too simplistic to yield quantitative results.

This concern is based on the requirement that all of the redox reactions calculated for this system are written (in the thermodynamic database used by the code) in terms of O_2 (Reactions a–c). This assumes that O(-II) is being oxidized to O(net 0) as NO_3^- is destroyed. This may not be a good assumption for such a complex system (i.e., where energetic particles and short-lived radiologic species are present). The implication of this assumption is that the increase in pH caused by the loss of nitrogen or nitrogen oxides would not depend on the identity of the nitrogen species leaving the system (Figures 11 and 12). However, writing the half-cell reactions (a'–c') suggests that there could be a significant difference in how the pH changes depending on which nitrogen species is lost to the system (see list of reactions below for more details).

Thus the conclusion at this point is that we need to understand the system better before this pH model can be used as supporting evidence for a process to adjust the pH during reactor operation. Further, when the results of this model are presented, a qualification should be added stating that the results are semiquantitative (i.e., a "step" toward understanding the real system).

Our ongoing work that will help resolve this issue includes conducting experimental studies (measuring gas compositions from relevant solutions under irradiation) and refining the thermodynamic model to account for more complex redox reactions.

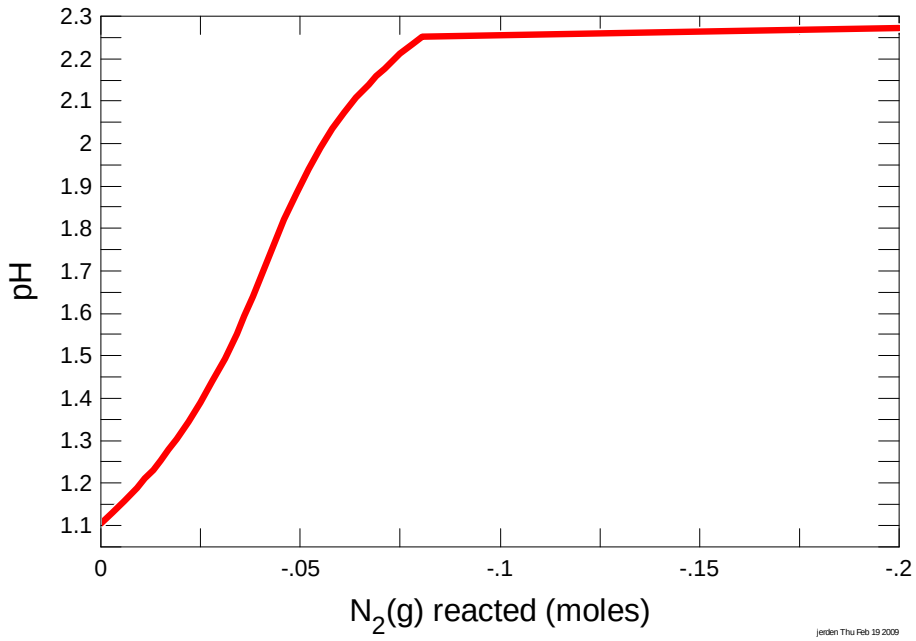

FIGURE 11 $N_2(g)$ "Negative" Titration [The reason the starting concentration of NO_3^- is below 2 molal is because approximately 0.2 molal $UO_2NO_3^+$ is also present in the solution (not shown).]

The key reactions influencing the pH are as follows:

$$NO_3^- + H^+ \rightarrow 0.5N_2(g) + 0.5H_2O(L) + 1.25O_2(aq) \quad \text{(a)}$$

$$NO_3^- + H^+ \rightarrow NO(g) + 0.5H2O(L) + 0.75O2(aq) \quad \text{(b)}$$

$$NO_3^- + H^+ \rightarrow NO_2(g) + 0.5H2O(L) + 0.25O2(aq) \quad \text{(c)}$$

The half-cell reactions are as follows:

$$NO_3^- + 5e^- + 6H+ \rightarrow 0.5N_2(g) + 3.0H_2O(L) \quad \text{(a′)}$$

$$NO_3^- + 3e^- + 4H^+ \rightarrow NO(g) + 2.0H_2O(L) \quad \text{(b′)}$$

$$NO_3^- + e^- + 2H^+ \rightarrow NO_2(g) + H_2O(L) \quad \text{(c′)}$$

For more details on the reactions used in the model see Section 4.3, List of Selected Reactions.

These models calculate the equilibrium conditions and speciation at every reaction step and therefore do not account for the details of the real system (kinetics, actual mass losses). The starting conditions for these models are 1 L of 1 mol uranyl nitrate + 0.1 mol nitric acid at 80°C.

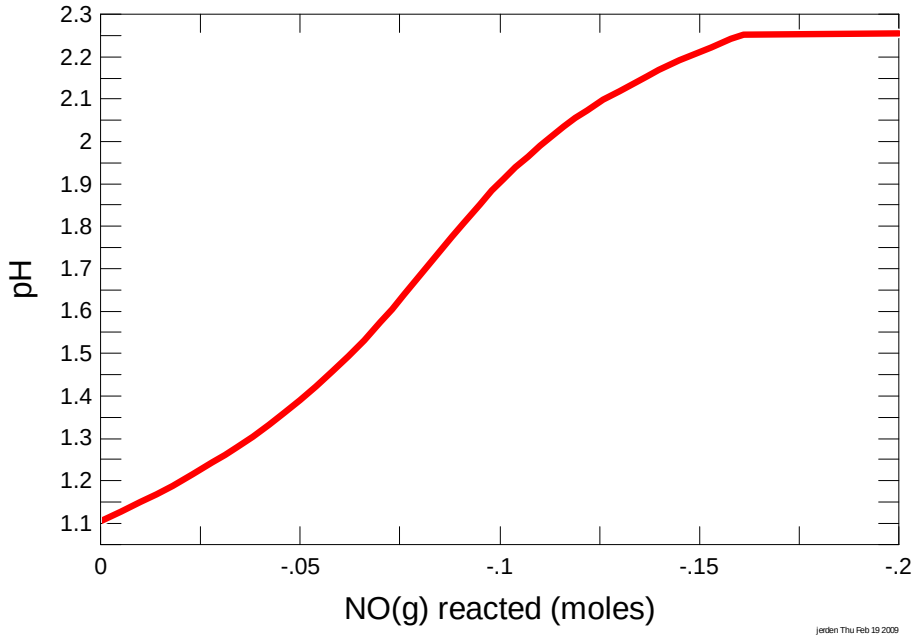

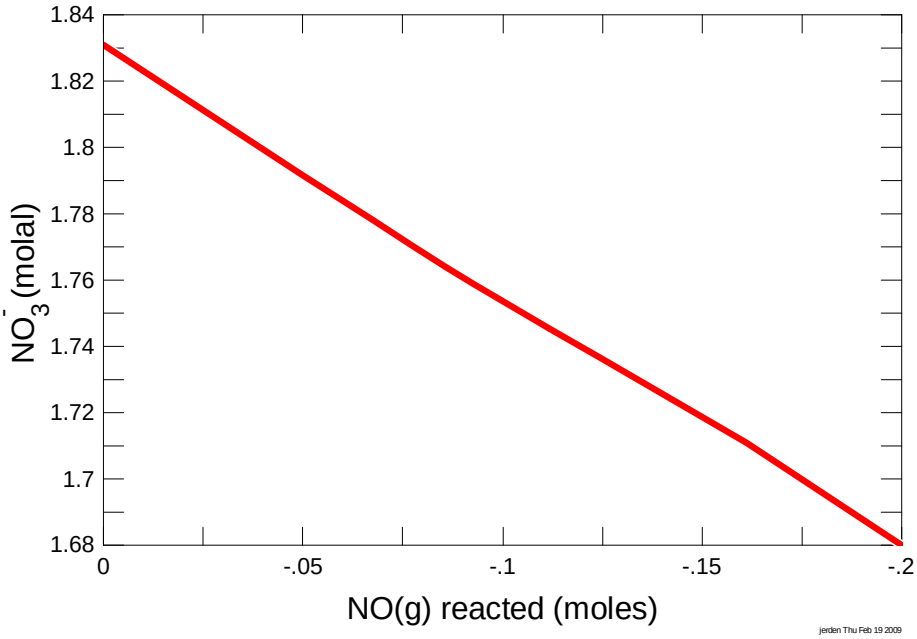

FIGURE 12 NO(g) "Negative" Titration [Note the pH plateau indicates precipitation of uranyl oxide hydrate. These results are identical to those found in the case where NO_2(g) is titrated out of the system. The reason that the starting concentration of NO_3^- is below 2 molal is because approximately 0.2 molal $UO_2NO_3^+$ is also present in the solution (not shown).]

4.2.1 Modeling Scenarios

(a) "Titrating" $NO_2(g)$ and $N_2(g)$ out of the solution: Note the pH plateau indicates the onset of uranyl oxide hydrate precipitation.

(b)"Titrating" $H_2O(g)$ out of the solution: Neither nitrogen nor nitrogen oxide gas is titrated out of the system for this model. The pH change is due only to the loss of $H_2O(g)$ (see Figure 13). Since this is an equilibrium model, it essentially simulates the evaporation of water from the system. This model was purposely taken to the extreme (half of the original water mass was titrated out) to show that, even in this case, the effect on pH is minor (starting solution = 1 L of 1 mol uranyl nitrate + 0.1 mol nitric acid at 80°C).

These simple equilibrium models suggest that the loss of nitrogen or nitrogen oxide gas will probably have a much stronger effect on the pH of the solution than a decrease in the mass of the solution would. However, since kinetic effects are not accounted for, these results should be viewed only as possibly being informative calculations rather than as process simulations.

4.3 LIST OF SELECTED REACTIONS

The following is a list of selected speciation and redox reactions (focused on nitrogen species) that are included in the model. The list of reactions is roughly ordered by oxidation state; it starts with N(V) species and works down to N_2 (accounting for acid dissociation reactions and gas solubilities along the way). The thermodynamic code solves a matrix of mass and charge balance equations that are determined by the equilibrium constants for the reactions listed below (not all reactions in the model are shown). By "titrating" nitrogen or nitrogen oxide out of the system, these reactions are "pulled" in a direction that favors a decrease in the hydrogen ion concentration/activity (see overall Reactions a and b). Also included at the end of Section 4.3 are Eh versus pH diagrams that summarize the redox relationships between key nitrogen species (see Figure 14).

$$UO_2(NO_3)_2 \leftrightarrow UO_2^{++} + 2NO_3^- \quad (1)$$

$$HNO_3(aq) \leftrightarrow H^+ + NO_3^- \quad (2)$$

$$HNO_3(aq) \leftrightarrow HNO_3(g) \quad (3)$$

$$NO_3^- + H^+ \leftrightarrow NO_2(aq) + 0.25O_2(aq) + 0.5H_2O(L) \quad (4)$$

Redox Reaction 4: N(V)/N(IV) written in terms of half-cell reactions:

$$NO_3^- + e^- + 2H^+ \leftrightarrow NO_2(aq) + H_2O(L) \quad (4a)$$

$$0.5H_2O(L) \leftrightarrow 0.25O_2(aq) + e^- + H^+ \quad (4b)$$

$$NO_3^- + H^+ \leftrightarrow NO_2(aq) + 0.25O_2(aq) + 0.5H_2O(L)$$

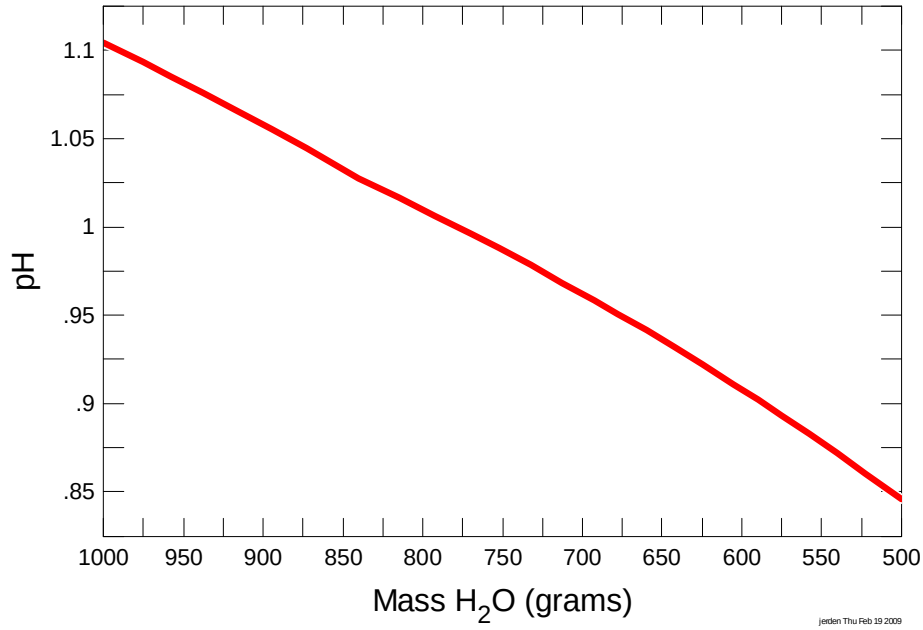

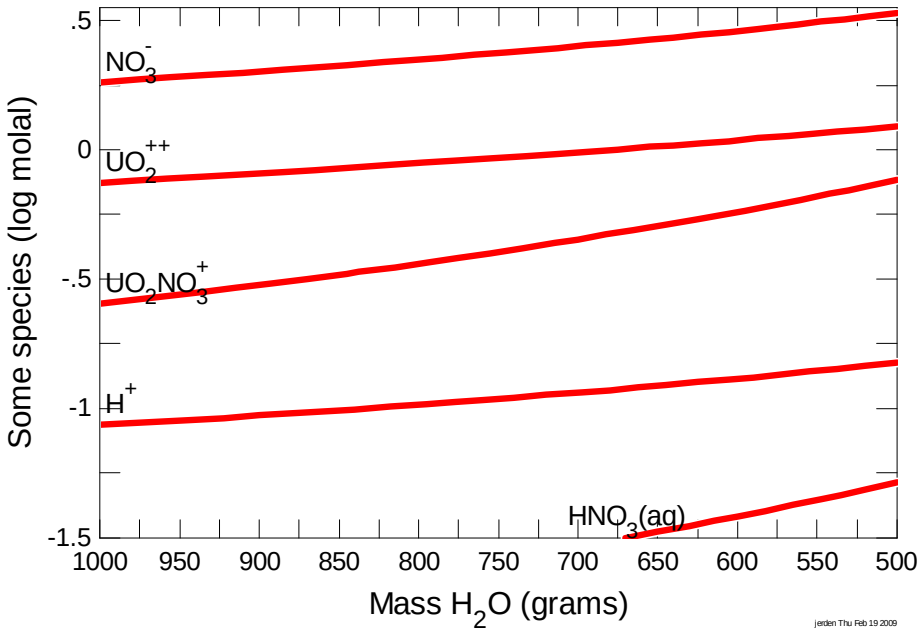

FIGURE 13 $H_2O(g)$ "Negative" Titration

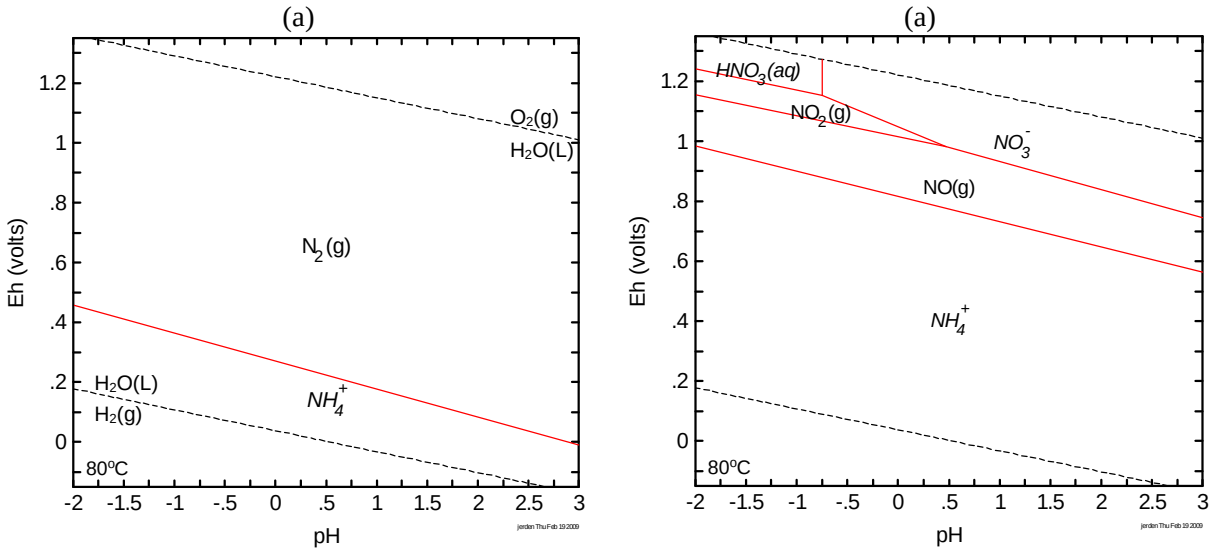

FIGURE 14 Redox Relationships between Species [In this case, the redox relationships between nitrogen species are shown in Eh versus pH diagrams, where Eh is the redox potential of the bulk solution (accounts for all redox couples in equilibrium) relative to the standard hydrogen electrode ($H^+(aq) + 2e^- \rightarrow 0.5H_2(g)$: Standard potential = 0). (a) The relationship is calculated for a case where the formation of $N_2(g)$ is not kinetically inhibited. (b) The relationship is calculated for a case where $N_2(g)$ is assumed to be kinetically inhibited from forming.]

$$NO_2(aq) \leftrightarrow NO_2(g) \tag{5}$$

$$2NO_2(aq) \leftrightarrow N_2O_4(aq) \tag{6}$$

$$N_2O_4(aq) \leftrightarrow N_2O_4(g) \tag{7}$$

$$NO_2(aq) + 0.5H_2O \leftrightarrow NO_2^- + 0.25O_2(aq) + H^+ \tag{8}$$

Redox Reaction 8: N(IV)/N(III) written in terms of half-cell reactions:

$$NO_2(aq) + e^- \leftrightarrow NO_2^- \tag{8a}$$

$$0.5H_2O(L) \leftrightarrow 0.25O_2(aq) + e^- + H^+ \tag{8b}$$
$$NO_2(aq) + 0.5H_2O(L) \leftrightarrow NO_2^- + 0.25O_2(aq) + H^+$$

$$NO_2^- + H^+ \leftrightarrow HNO_2(aq) \tag{9}$$

$$HNO_2(aq) \leftrightarrow HNO_2(g) \tag{10}$$

$$NO_2^- + H^+ \leftrightarrow NO(aq) + 0.25O_2(aq) + 0.5H_2O \tag{11}$$

Redox Reaction 11: N(III)/N(II) written in terms of half-cell reactions:

$$NO_2^- + e^- + 2H^+ \leftrightarrow NO(g) + H_2O(L) \quad (11a)$$

$$0.5H_2O \leftrightarrow 0.25O_2(aq) + e^- + H+ \quad (11b)$$
$$NO_2^- + H^+ \leftrightarrow NO(aq) + 0.25O_2(aq) + 0.5H_2O(L)$$

$$NO(aq) \leftrightarrow NO(g) \quad (12)$$

$$2NO(aq) \leftrightarrow N_2(aq) + O_2(aq) \quad (13)$$

Redox Reaction 13: N(II)/N(net 0) written in terms of half-cell reactions:

$$2NO(g) + 4e^- + 4H+ \leftrightarrow N_2(g) + 2H_2O \quad (13a)$$

$$2H_2O(L) \leftrightarrow O_2(aq) + 4e^- + 4H^+ \quad (13b)$$
$$2NO(aq) \leftrightarrow N_2(aq) + O_2(aq)$$

$$N_2(aq) \leftrightarrow N_2(g) \quad (14)$$

Other Important Reactions:

$$H_2O(L) \leftrightarrow H_2O(g) \quad (15)$$

$$H_2O(L) \leftrightarrow H_2(aq) + 0.5O_2(aq) \quad (16)$$

Redox Reaction 16: O(-II) to O(net 0) written in terms of half-cell reactions:

$$H_2O(L) \leftrightarrow 0.5O_2(g) + 2e^- + 2H^+ \quad (16a)$$

$$2H^+ + 2e^- \leftrightarrow H_2(aq) \quad (16b)$$
$$H_2O(L) \leftrightarrow H_2(aq) + 0.5O_2(aq)$$

$$O_2(aq) \leftrightarrow O_2(g) \quad (17)$$

$$H_2(aq) \leftrightarrow H_2(g) \quad (18)$$

$$H_2O_2 \leftrightarrow 0.5O_2(aq) + H_2O(L) \quad (19)$$

Redox Reaction 19: O(III) to O(net 0) written in terms of half-cell reactions:

$$H_2O_2 + 2e^- + 2H^+ \leftrightarrow 2H_2O(L) \tag{19a}$$

$$H_2O(L) \leftrightarrow 0.5O_2(g) + 2e^- + 2H^+ \tag{19b}$$
$$H_2O_2 \leftrightarrow 0.5O_2(aq) + H_2O(L)$$

$$Fe + 3H^+ + 0.75O_2(aq) + NO_3^- \rightarrow FeNO_3^{2+} + 1.5H_2O(L) \tag{20}$$

Redox Reaction: Fe(0)/Fe(III) written in terms of half-cell reactions:

$$Fe + NO_3^- \leftrightarrow 3e^- + FeNO_3^{++} \tag{20a}$$

$$3H^+ + 0.75O_2(g) + 3e^- \leftrightarrow 1.5H_2O(L) \tag{20b}$$
$$Fe + 3H^+ + 0.75O_2(aq) + NO_3^- \leftrightarrow FeNO_3^{2+} + 1.5H_2O(L)$$

Reactions Counteracting pH Increase:

$$FeNO_3^{2+} + 3H_2O(L) \leftrightarrow Fe(OH)_3(s) + 3H^+ + NO_3^- \tag{21}$$

$$UO_2^{2+} + 3H_2O(L) \leftrightarrow UO_3{:}2H_2O(s) + 2H^+ \tag{22}$$

$$UO_2^{2+} + 4H_2O(L) + H_2O_2 \leftrightarrow UO_2O_2{:}4H_2O(s) + 2H^+ \tag{23}$$

5 PRELIMINARY RESULTS FROM URANYL PEROXIDE PRECIPITATION EXPERIMENTS

5.1 INTRODUCTION

During operation of the MIPS, hydrogen peroxide will be produced by the radiolysis of water. The rate of H_2O_2 generation is proportional to the energy absorbed by the water. If the steady- state concentration of H_2O_2 is high enough, the solid uranyl peroxide may precipitate. Excessive amounts of this precipitate would lower the concentration of uranium in the fuel and produce local "hotspots" and might induce corrosion. The purpose of this study is to determine the stability of uranyl peroxide for conditions relevant to the MIPS.

5.2 EXPERIMENT

Hydrogen peroxide was added to 100 mL of 0.63 mol/L (150 g/L) uranyl nitrate solution at pH = 1 such that the hydrogen peroxide concentration upon the addition was 0.4 mol/L (see Experiments 1, 2, and 3 in Table 3). The addition of hydrogen peroxide diluted the uranium in the samples to 0.57 mol/L (135.7 g/L).

Upon addition of the hydrogen peroxide to the fuel stimulant, a fine-grained uranyl peroxide solid precipitated immediately. This procedure was done for three separate experiments. The concentration of uranium for these samples was measured by inductively coupled mass spectrometry for each sample at three different time intervals. Two of the experiments were run at 80°C, while one was run at 25°C. All of the experiments were performed in Teflon screw-cap vessels. One of the experimental vessels (3) contained a layer (1 g) of 304L stainless steel granules.

In three other experiments (under-saturation tests), 0.63 g of previously precipitated uranyl peroxide (probably $UO_2O_2{:}4H_2O$) was washed three times in deionized water and added to 100 mL of sodium nitrate solution at pHs of 0, 1.1, and 2.1 (see Experiments 4, 5, and 6, respectively, in Table 3).

5.3 PRELIMINARY EXPERIMENTAL RESULTS

The results of the experiments and the experimental conditions are shown in Table 3. The precipitation of uranyl peroxide solid decreased the uranium concentration in the fuel solution to 0.2 M (47.6 g/L) when no steel was present and to 0.46 M (109.5 g/L) when steel was present. Within 24 hours at 80°C, the uranium in the simulated fuel increased to 0.48 M (114.2 g/L), and within 6 days at 80°C, the simulated fuel reached a concentration of 0.57 M (135.7 g/L). The dissolution kinetics for the uranyl peroxide solid and/or the H_2O_2 decomposition rates for the lower-temperature samples were slower, reaching a uranium concentration of 0.48 M (114.2 g/L) after 6 days. The sample with a steel layer showed a smaller initial decrease in its uranium concentration, but then the concentration remained relatively constant for the 6-day experimental

TABLE 3 Concentrations (by Inductively Coupled Plasma Mass Spectrometry) and Experimental Conditions for Uranyl Peroxide Stability Tests

Test	Time Reacted (days)	pH	U (mol)	T (°C)
1	Initial	1	0.21	80
1	1	1	0.48	80
1	6	1	0.57	80
2	Initial	1	0.46	80
2	1	1	0.44	80
2	6	1	0.45	80
3	Initial	1	0.19	25
3	1	1	0.26	25
3	6	1	0.48	25
4	Initial	0	4.17E-05	80
4	1	0	3.64E-04	80
4	6	0	1.68E-02	80
5	Initial	1	1.74E-06	80
5	1	1	8.28E-03	80
5	6	1	2.13E-02	80
6	Initial	2	5.84E-07	80
6	1	2	2.31E-04	80
6	6	2	4.15E-02	80

period. This is believed to have been caused by the chemisorption or reductive precipitation of uranium on the steel surface, which turned from shiny silver to black during the duration of the experiment.

These findings are preliminary results from ongoing experiments that will be used to determine the stability of uranyl peroxide under conditions relevant to the MIPS. The key results so far suggest that a uranyl peroxide solid could possibly form under certain conditions (depending on the steady-state concentration of H_2O_2 during reactor operation). However, due to the rate of destruction of H_2O_2 at the relevant temperature (80°C), it is likely that the fuel solution will remain undersaturated with respect to uranyl peroxide as long as the solution pH remains <2. But again, more experimental data are needed to verify these findings.

5.4 MODELING RESULTS

The uranyl peroxide stability calculations were made using the thermodynamic by using the codes OLI ESP and “Geochemist’s Workbench,” Release 3.0 of GWB. The results from the two codes agree. The thermodynamic database used for modeling was compiled from literature sources. In general, both modeling codes use a Gibb’s free energy minimization technique to determine the equilibrium state of the system of interest. More specifically, the codes use the

equilibrium constants for a set of basis reactions to solve a matrix of mass and charge balance equations. Results from these calculations feed into an iterative algorithm that converges on a unique equilibrium state for the multicomponent, multiphase system of interest.

The stability of $UO_2O_2{:}4H_2O$ as a function of hydrogen peroxide concentration and pH is shown in Figure 15. This diagram is plotted for a uranium concentration of 0.63 M uranyl nitrate, and the pH is varied as HNO_3. This diagram implies that at pH = 1, the steady-state concentration of uranyl peroxide would have to be approximately $1 \times 10^{-4.5}$ M for the fuel solution to become saturated with respect to uranyl peroxide.

Figure 16 shows two modeling scenarios in which 0.63 mol uranyl nitrate is assumed while the pH is varied as HNO_3. The plots show the amount of uranyl peroxide that would precipitate for a steady-state H_2O_2 concentration of 1×10^{-3} (a) and 1×10^{-6} (b). These model runs indicate that at an H_2O_2 concentration of 1×10^{-6}, the fuel solution would not become saturated with respect to uranyl peroxide at pH = 1, but it would become saturated if the pH increased to around 2. Figure 16 also shows the speciation of uranium within the fuel as a function of pH. Note that the concentration of uranium is predicted to decrease dramatically when the uranyl oxide hydrate schoepite precipitates at a pH of around 3.0, indicating that such a condition is to be avoided during MIPS operation.

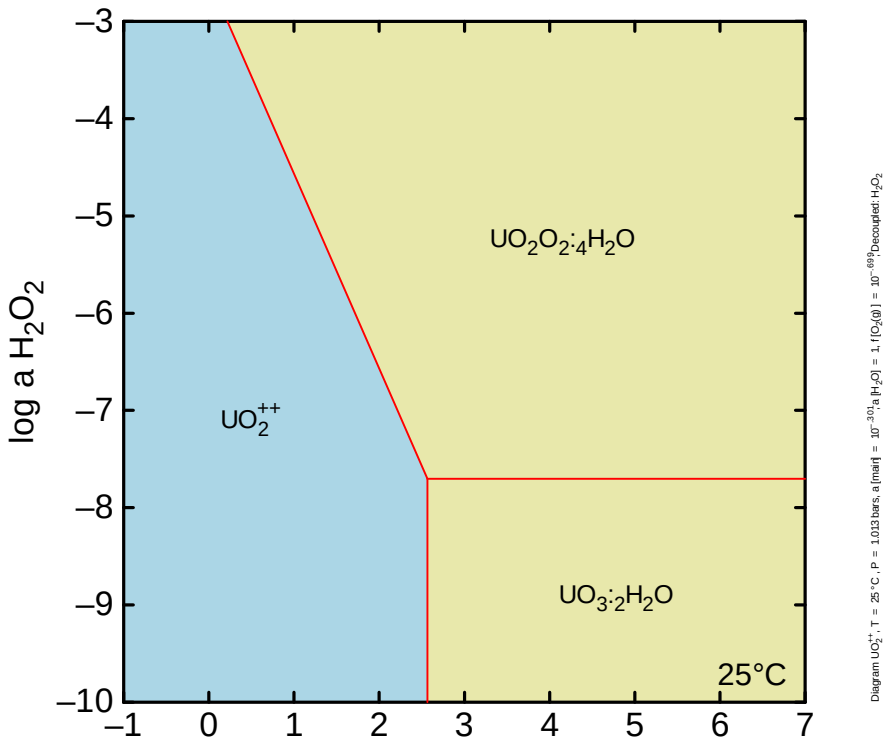

FIGURE 15 Activity Diagram Showing the Stability Field of Uranyl Peroxide ($UO_2O_2{:}4H_2O$) as a Function of H_2O_2 concentration and pH (The uranium concentration for this diagram is 0.63 M, and the pH is adjusted as HNO_3.)

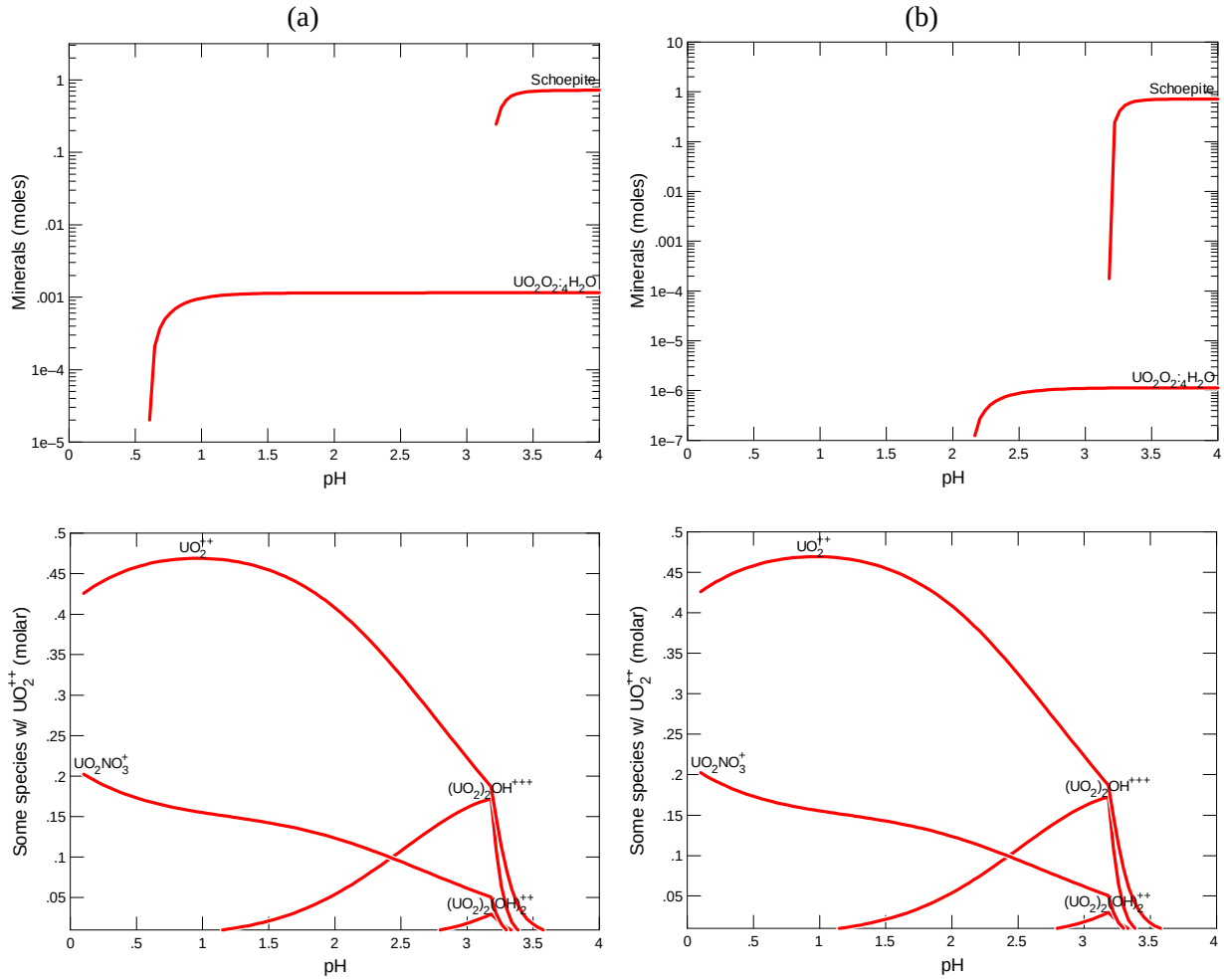

FIGURE 16 Solid (top) and Aqueous (bottom) Speciation Diagrams for (a) 1×10^{-3} M and (b) 1×10^{-6} M H_2O_2 Steady-State Concentration (Both model runs are for 0.63 M uranium, and the pH is adjusted as HNO_3.)

6 CONCLUSION

Each of the four studies discussed represents ongoing work that will become more quantitative as the project continues. These modeling and preliminary experimental studies are useful in pointing out what type of data are needed to produce a more realistic working model of the MIPS system. As these projects continue, they will produce the type of results needed to determine the optimal conditions and materials for both reactor operation and molybdenum extraction from the fuel. The future work for each project is identified in Section 1.3.

7 REFERENCES

Baes, C.F., Jr., and R.E. Mesmer, 1976, *The Hydrolysis of Cations*, Wiley, New York, N.Y.

Bard, A.J., et al., 1985, *Standard Potentials in Aqueous Solution*, Dekker, New York, N.Y.

Faure, G., 1998, *Principles and Applications of Geochemistry*, Prentice Hall, Upper Saddle River, N.J.

Lindsay, W.L., 1979, *Chemical Equilibria in Soils*, Wiley Interscience.

Wolery, T.J., and S.A. Daveler, 1992, EQ6, *A Computer Program for Reaction Path Modeling of Aqueous Geochemical Systems: Theoretical Manual, User's Guide, and Related Documentation (Version 7.0)*, Lawrence Livermore National Laboratory Report UCRL-MA-110662 PT IV.

Chemical Science and Engineering Division
Argonne National Laboratory
9700 South Cass Avenue, Bldg. 205
Argonne, IL 60439-4837

www.anl.gov

Argonne National Laboratory is a U.S. Department of Energy
laboratory managed by UChicago Argonne, LLC